# A Preliminary Study of RF Propagation for High Data Rate Brain Telemetry

Mariella Särestöniemi[1,2], Carlos Pomalaza-Raez[3], Kamran Sayrafian[4], Teemu Myllylä[1,5], Jari Iinatti[1]

[1] Centre for Wireless Communications, University of Oulu, Finland
[2]Research Unit of Medical Imaging, Physics and Technology, Faculty of Medicine, University of Oulu, Finland
[3] Purdue University of Technology, USA
[4]National Institute of Standards and Technology, Maryland, USA
[5]Optoelectronics and Measurement Techniques Research Unit, Faculty of Information Technology and Electrical Engineering, University of Oulu, Finland
Corresponding Author: mariella.sarestoniemi@oulu.fi

**Abstract.** This paper presents the preliminary results of a study on the radio frequency (RF) propagation inside the human skull at several Industrial, Scientific and Medical (ISM) and ultrawideband UWB frequencies. These frequency bands are considered as possible candidates for high data rate wireless brain telemetry. The study is conducted using a high-resolution 3D computational model of the human head. Power flow analysis is conducted to visualize propagation inside the brain for two different on-body antenna locations. Furthermore, channel attenuation between an on-body directional mini-horn antenna and an implant antenna at different depths inside the brain is evaluated. It is observed that radio frequency propagation at 914 MHz sufficiently covers the whole volume of the brain. The coverage reduces at higher frequencies, specially above 3.1 GHz. The objective of this comparative analysis is to provide some insight on the applicability of these frequencies for high data rate brain telemetry or various monitoring, and diagnostic tools.

**Keywords:** Brain Computer Interface, Brain Monitoring, Frequency Channel Response, Implant Communications, In-body Propagation

## 1 Introduction

There has been a growing interest in the development of non-invasive acute brain injury detection and continuous monitoring systems in recent years [1]-[12]. Advances in microelectronics is also contributing to significant progress in invasive monitoring systems such as intra cranial pressure and brain oxygenation monitoring [5]-[8]. In addition, Brain Computer Interface (BCI) as a multidisciplinary research area has drawn considerable attention due to its attractive and transformative applications across many verticals in wireless communications including E-Health [1],[2], [3], [9]. Low-power,

reliability, and security are essential requirements for wireless monitoring of the brain signals. Some BCI applications may require wireless links that can support high data rates reaching 100 Mbps [1], [2]. In order to meet these requirements, in-depth propagation studies at various frequency bands are essential in the design of a wireless brain telemetry system.

Wireless propagation inside the human body at different frequency bands including Industrial, Scientific and Medical (ISM), Wireless Medical Telemetry Service (WMTS), Ultra WideBand (UWB), and Medical Device Radio Communications Service (MedRadio) is an attractive and challenging topic of research in Body Area Networks [13]-[18]. However, there are only few such studies in the literature for brain implant communication [16]-[22], [23], [24]. Most of the existing studies are based on simple tissue-layer models. Those models are more relevant for applications where the brain implant is relatively close to the skull. For wireless monitoring applications where the implant could be located deeper inside the brain, it is important to study propagation using more realistic models of the human head. It is also necessary to identify which frequency bands would be suitable for different brain monitoring or implant communication applications. This identification should take into the account all desirable requirements for the wireless communication link. The main objective of this paper is to study radio waves propagation inside the human skull at several frequency bands. The novelty of this paper compared to other brain propagation studies in the literature is the use of a more accurate computational model of the human head, and a directional on-body antenna which allows for evaluation at several frequency bands appropriate for medical applications.

The rest of this paper is organized as follows: Section II presents the simulation environment and the antennas used in this study. Section III presents the simulation results for two different on-body antenna locations, including power flow analysis and channel characteristics evaluations. Conclusions and future work are provided in Section IV.

## 2 Simulation Environment and Antenna Models

### 2.1 Simulation Model

This study is conducted using Simulia CST studio suite[1] 3D electromagnetic simulation software [25] which is based on Finite Integration Technique (FIT). The anatomical 3D head model from the CST's Hugo voxel-based body model shown in Fig. 1a has been used for simulation purposes. Hugo voxel-based head model includes brain tissue structure with separate grey and white matters as depicted in the 2D cross section in Fig. 1b. The frequency-dependent dielectric properties of the voxel tissues are obtained using four-pole Cole-Cole modeling described in [26]. Relative permittivity $\varepsilon_r$ and conductivity $p$ of the most relevant tissues in the head are presented in Table 1 [27].

[1] Commercial products mentioned in this paper are merely intended to foster understanding. Their identification does not imply recommendation or endorsement by National Institute of Standards & Technology

a) 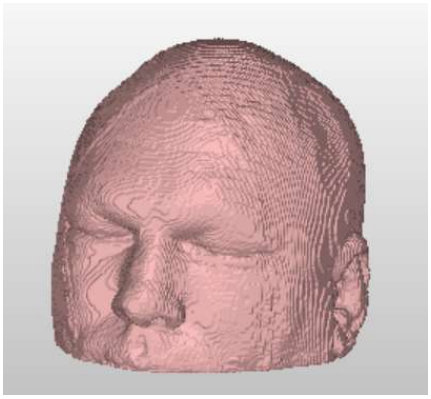 b) 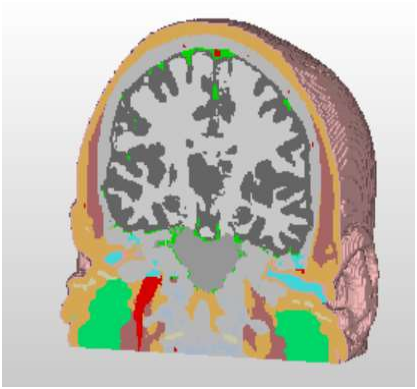

**Fig. 1.** a) Hugo voxel model b) Cross-section of the head model

**Table 1.** Dielectric properties of the head tissues at several frequencies

| **Tissue** | 0.914 GHz $\varepsilon_r$ / p [S/m] | 2.45 GHz $\varepsilon_r$ / p [S/m] | 3.1 GHz $\varepsilon_r$ / p [S/m] | 4.0 GHz $\varepsilon_r$ / p [S/m] | 5.8 GHz $\varepsilon_r$ / p [S/m] |
|---|---|---|---|---|---|
| Skin | 41.3 / 0.9 | 38.0 / 1.46 | 37.4 / 1.79 | 36.6 / 2.34 | 35.1/3.72 |
| Fat | 11.3 / 0.11 | 10.8 / 0.27 | 10.6 / 0.40 | 10.4 / 0.50 | 9.86/8.32 |
| Muscle | 55.0 / 0.95 | 52.7 / 1.74 | 51.8 / 3.02 | 50.8 / 3.02 | 48.5/4.96 |
| Skull bone | 20.8 / 0.34 | 18.5 / 0.81 | 17.8 / 1.04 | 16.9 / 1.40 | 15.4/2.15 |
| Brain grey matter | 52.7 / 0.95 | 48.9 / 1.81 | 47.9 / 2.30 | 46.6 / 3.09 | 44.0/4.99 |
| Brain white matter | 38.8 / 0.60 | 36.2 / 1.21 | 35.4 / 1.57 | 34.5 / 2.14 | 32.6/3.49 |

### 2.2 Mini-horn Antenna

A directional bio-matched mini-horn antenna, shown in Fig. 2, has been used for our evaluations in this paper. The mini-horn antenna originally presented in [28] has been modified and updated for this study in order to obtain better matching with the voxel-based head model [11]. The modified structure has dimensions $h$=2.7 cm and $d$=1.8 cm (see Fig. 2). The antenna is composed of water-filled holes which mimics the frequency-dependent relative permittivity of the underlying tissue over its entire bandwidth. The bio-matched mini-horn antenna has been designed to operate while tightly attached to the skin surface. Although the resolution of the Hugo voxel model is high, pixelization on the head surface could lead to air gaps between the antenna and the skin as explained in [11]. This effects negatively on the antenna matching and hence the resulting channel simulations as shown in [11]. To alleviate this problem, the air gaps have been replaced by a thin layer of skin between the antenna and the surface of the head where the antenna is placed [11]. This “smoothing layer” creates a better and more realistic contact between the antenna and the scalp. Further details of the antenna structure can be found in [28].

For RF propagation evaluation, two antenna locations on the surface of the head have been considered: Location 1) on the side, and Location 2) on the top, see Fig. 3 a-b. These locations are selected due to their different propagation environments. At location 1, there is a relatively thick muscle tissue below the mini-horn antenna; however, no such muscle exists at location 2. Fig. 4. presents the antenna reflection coefficients, i.e., $S_{11}$ parameter, of the mini-horn antenna after adjustment with the smoothing layers at locations 1 and 2.

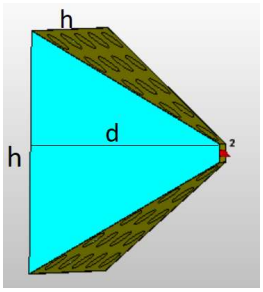


**Fig. 2.** Mini-horn on-body antenna designed for in-body communication.

a) 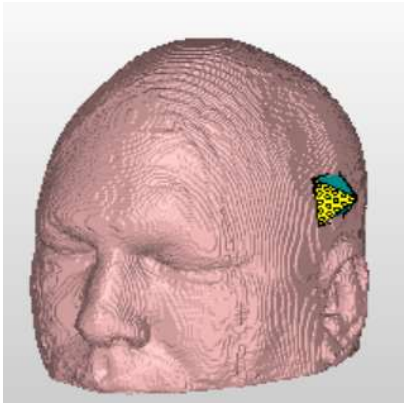 b) 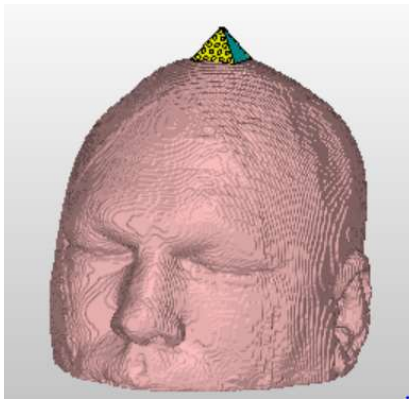

**Fig. 3.** On-body antenna locations: a) Location 1 (above the temporal bone on the left side), b) Location 2 (top of the head)

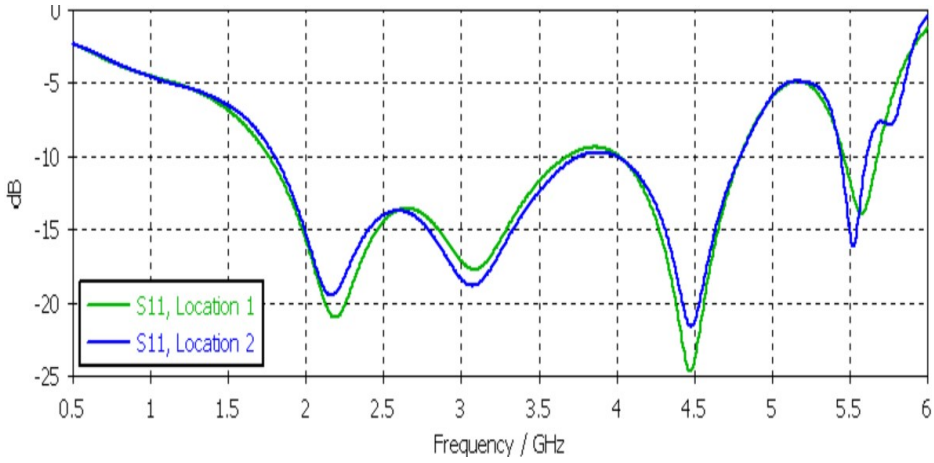


**Fig. 4.** Reflection coefficient of the mini-horn antenna placed on Hugo's scalp at locations 1 and 2

### 2.3 Implant Antenna

The implant antenna used in this study is a double-loop UWB antenna originally introduced in [29] for capsule endoscopy application. It has a cylindrical shape with a size of 11 mm by 15 mm as shown in Fig. 5. Although this antenna might not be applicable for practical brain implants, its capability to operate over a large bandwidth (i.e., 1-6 GHz) will allow us to carry out the preliminary RF propagation study in this paper. In addition to the 1-6 GHz frequency range which this antenna has been designed for, it offers reasonable performance at the ISM (902−928) MHz band as well.

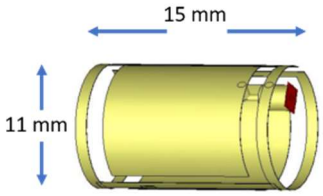


**Fig. 5.** UWB implant antenna

The locations where this antenna has been placed inside the brain to measure the forward channel coefficients as well as power flow values are shown in Fig. 6a-b. They are marked as points A, B, C, D, E and F. Fig. 6a and Fig. 6b show these locations when the mini-horn antenna is at location 1 and 2, respectively. These points represent various propagation depths of A=1.6 cm, B=3.0 cm, C=4.3 cm, D=5.3 cm, E=6.3 cm and F=7.3 cm. The locations also represent different propagation environments including muscle layers and white/grey matter compositions inside the brain. The authors

acknowledge that these locations may not necessarily indicate practical locations for medical implants.

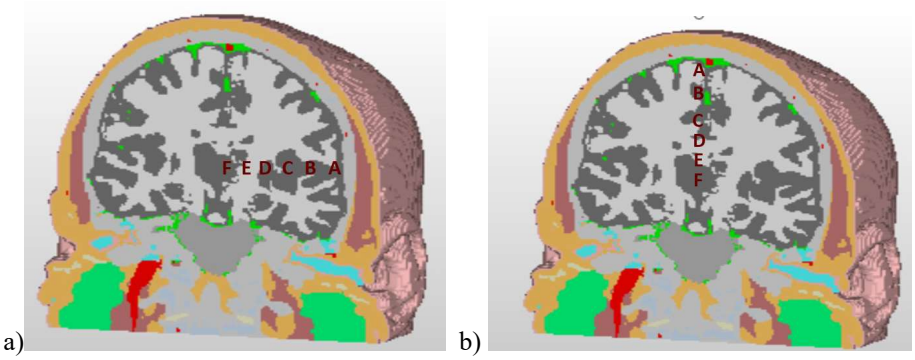


**Fig. 6.** Implant locations for which the power flow and channel attenuation have been evaluated a) on-body antenna at location 1 and b) on-body antenna at location 2

The S11 parameter of this antenna while located at point A is presented in Fig. 7. Further details of the antenna structure, radiation pattern, as well as Specific Absorption Rate (SAR) have been studied in [29].

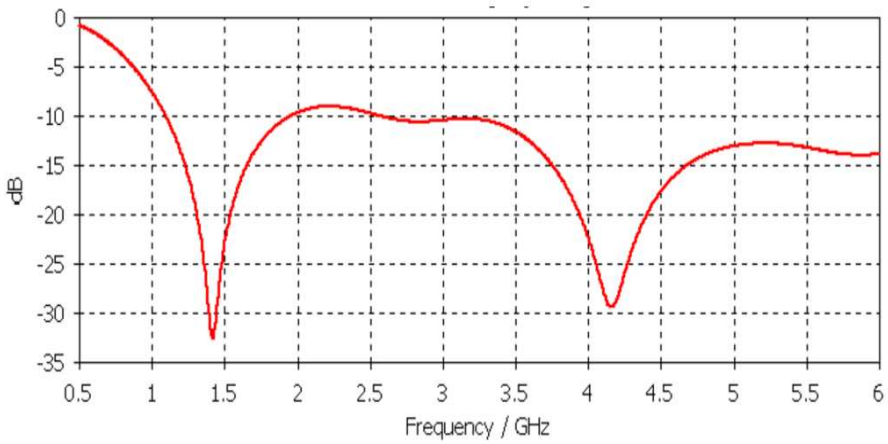


**Fig. 7.** Reflection coefficient of the implant antenna inside the brain tissue

# 3 Simulation Results

## 3.1 Power Flow Results for the On-body Antenna Location 1

In-body propagation results at different frequencies using the notion of power flow is presented in this section. Power flow is the time-averaged magnitude of the Poynting vector [26]. The Poynting vector represents the directional energy flux (the energy transfer per unit area per unit time) of an electromagnetic field. The flux of the Poynting Vector through a certain surface represents the total electromagnetic power flowing through that surface. Here, the power flow values (expressed in decibels) have been normalized so that 0 dB represents the maximum. Figs. 8a-e present the power flows (ranging from 0 to -65 dB) on the horizontal (left) and vertical (right) cross-sections of the brain at 915 MHz, 2.45 GHz, 3.1 GHz, 4.0 GHz, and 5.8 GHz, respectively. These figures correspond to location 1 of the mini-horn antenna. Power flow values at locations A, B, C, D, E and F are also provided in Table 2.

As observed in Fig. 8a, at 915 MHz, a good coverage is obtained throughout the whole volume of the head with power flow values well within the selected 65 dB range. At this frequency, the power flow values decrease gradually from -35 dB to -54 dB as the propagation depth increases from point A=1.6 cm to point F=7.3 cm. At 2.45 GHz, the power flow plots indicate coverage of only ¾ of the head volume (Fig. 8b). As expected, power loss in the brain tissue increases with higher frequencies and the size of the covered volume specially declines for UWB. The power flow plots at 3.1 GHz and 4 GHz indicate a coverage of half and almost 1/3 of the brain volume respectively (see Figs. 8c-d). Again, power flow values gradually decrease as the propagation distance increases (Table 2).

One might note that at point A, power flow at 914 MHz is smaller compared to its values at 2.45 GHz and 3.1 GHz. This is inconsistent with the fact that propagation loss is typically smaller at lower frequencies**.** However, as observed in Fig. 4, the reflection coefficient of the mini-horn antenna at 2.45 GHz is significantly better compared to 914 MHz. This results in larger power flow value at 2.45 GHz. However, as the propagation depth increases, higher power loss in the tissue at 2.45 GHz overcomes the reflection coefficients discrepancy and power flow values drop below their corresponding values for 914 MHz.

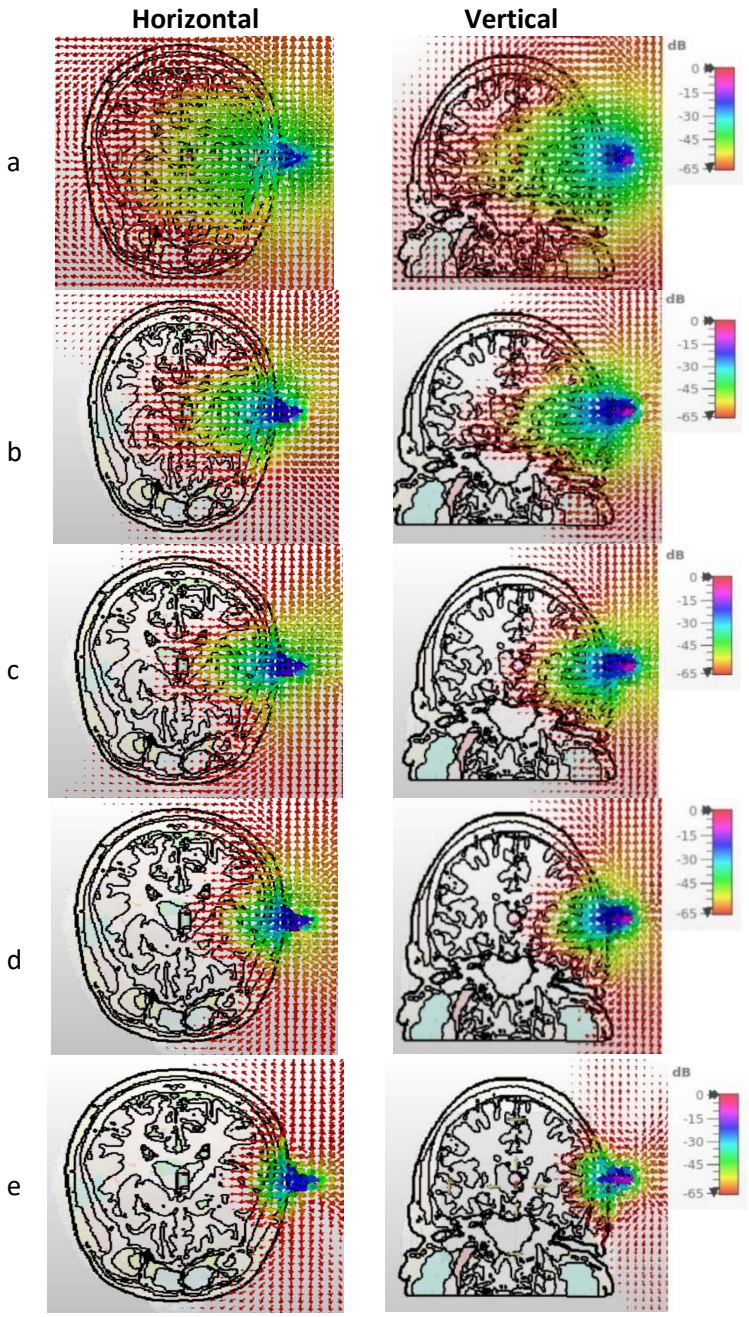


**Fig. 8.** Power flows from the mini-horn antenna at location 1 a) 914 MHz, b) 2.45 GHz, c) 3.1 GHz, d) 4.0 GHz, and e) 5.8 GHz

**Table 2.** Power flow values for on-body antenna location 1 at various depths

| **Location and distance from the surface** | **Frequencies** | | | | |
|---|---|---|---|---|---|
| | 0.914 GHz | 2.45 GHz | 3.1 GHz | 4.0 GHz | 5.8 GHz |
| A (1.6 cm) | -35 [dB] | -32 [dB] | -33 [dB] | -35 [dB] | -48 [dB] |
| B (3.0 cm) | -38 [dB] | -38 [dB] | -41 [dB] | -45 [dB] | -62 [dB] |
| C (4.3 cm) | -43 [dB] | -41 [dB] | -51 [dB] | -57 [dB] | -81 [dB] |
| D (5.3 cm) | -45 [dB] | -49 [dB] | -54 [dB] | -63 [dB] | -93 [dB] |
| E (6.3 cm) | -48 [dB] | -53 [dB] | -59 [dB] | -71 [dB] | -101 [dB] |
| F (7.3 cm) | -54 [dB] | -58 [dB] | -63 [dB] | -78 [dB] | -110 [dB] |

### 3.2 Channel Attenuation for the On-body Antenna Location 1

In this section, we evaluate the channel frequency responses between the mini-horn antenna at location 1 and the implant antenna when placed at locations A through F. The objective is to understand the impact of the propagation depth on the channel attenuation. The forward channel coefficients (S21) at locations A-F are presented in Fig. 9. Assuming that a maximum pathloss of 65 dB is tolerable in order to maintain a reliable communication link, it is observed that the channel attenuations at 914 MHz, 2.45 GHz, and 3.1 GHz are within the acceptable threshold for all considered propagation depths. Maximum attenuations for these frequencies (which occurs at location F) are -54 dB, -58 dB, and -63 dB, respectively. However, at 4 GHz, the channel attenuation is manageable only at the implant locations A-D. At implant locations E and F, a receiver with higher sensitivity would be required as channel attenuation for these locations are over 70 dB. At 5.8 GHz, only locations A and B experience channel attenuation within the 65 dB margin. These results are aligned with the power flow observations discussed in Section 3.1.

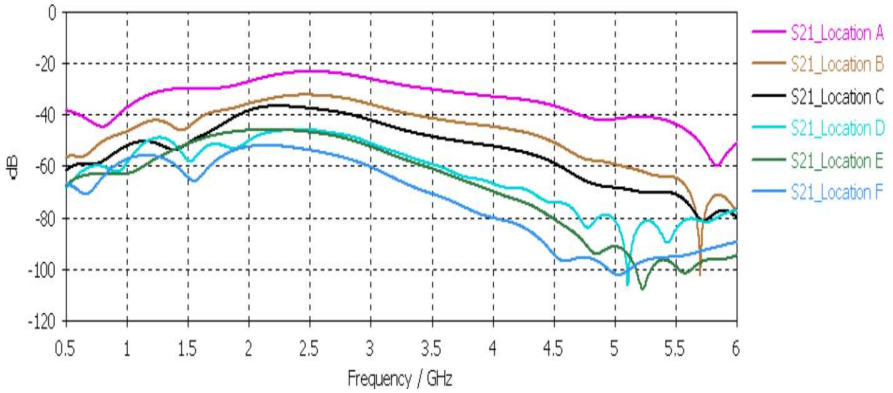


**Fig. 9.** Forward channel coefficient (S21) for different implant locations and mini-horn antenna location 1

### 3.3 Power Flow Results for the On-body Antenna Location 2

In this subsection, a similar propagation study is conducted for the on-body antenna location 2 (see Fig. 3b). For brevity, only the power flow results have been provided. Figs. 10a-d presents the power flows on the horizontal (left) and vertical (right) cross-sections of the brain at 915 MHz, 2.45 GHz, 3.1 GHz, and 5.8 GHz, respectively. The magnitude ranges from 0 to -65 dB similar to the on-body antenna location 1. Power flow values at locations A, B, C, D, E, and F are also provided in Table 3.

It is observed that the power flow values resulting from the on-body antenna location 2 are generally at higher levels compared to the antenna location 1. This is mostly due to the existence of the temporalis muscle which is a thick muscle layer on each side of the head filling the temporal fossa. This muscle directly sits on the propagation path from the antenna location 1. RF attenuation in the muscle tissue is typically high due to its dielectric properties [16]. Another reason for higher values of power flow from location 2 is the amount of grey matter that exist between the implant and the on-body antenna. Compared to the white matter in the brain tissue, the propagation loss in the grey matter is substantially higher due to its dielectric properties [16]. Since there is more grey matter on the propagation path between the implant and the on-body antenna location 1, the attenuation would be higher, resulting in relatively lower power flow values.

An interesting phenomenon is observed at 5.8 GHz for locations E and F. These locations are closer to the center of the brain. The power flow values at these locations unexpectedly increase, although propagation depth from the on-body antenna is higher. One possible explanation for this phenomenon is the existence of an alternate path for the radio waves to arrive at these points. As observed in Fig. 10e (vertical cross-section), a stronger flow through the nasal cavities could be the reason for better signal penetration to the middle of the brain. The possibility of surface propagation through this secondary route (i.e., nasal cavities) and constructive addition of the RF waves on this route with the waves penetrating directly from top of the skull could lead to higher power flow values at these locations for 5.8 GHz. Further studies would be necessary to verify this justification.

**Table 3.** Power flow values for on-body antenna location 2 at various depths

| **Location and distance from the surface** | **Frequencies** | | | | |
|---|---|---|---|---|---|
| | 0.914 GHz | 2.45 GHz | 3.1 GHz | 4.0 GHz | 5.8 GHz |
| A (1.6 cm) | -32 [dB] | -30 [dB] | -28 [dB] | -29 [dB] | -37 [dB] |
| B (3.0 cm) | -35 [dB] | -35 [dB] | -38 [dB] | -39 [dB] | -59 [dB] |
| C (4.3 cm) | -38 [dB] | -40 [dB] | -44 [dB] | -49 [dB] | -73 [dB] |
| D (5.3 cm) | -40 [dB] | -42 [dB] | -48 [dB] | -57 [dB] | -84 [dB] |
| E (6.3 cm) | -42 [dB] | -47 [dB] | -53 [dB] | -61 [dB] | -79 [dB] |
| F (7.3 cm) | -44 [dB] | -54 [dB] | -60 [dB] | -70 [dB] | -70 [dB] |

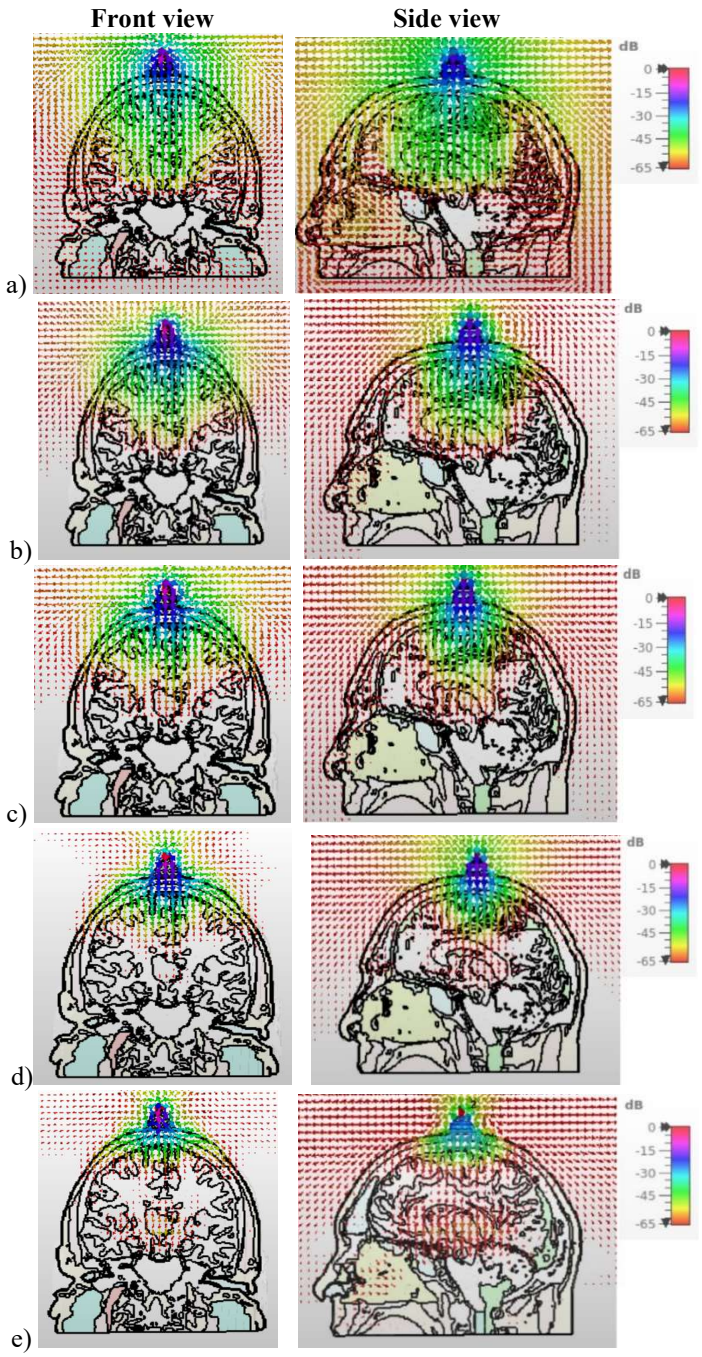


**Fig. 10.** Power flows from the mini-horn antenna at location 2 a) 914 MHz, b) 2.45 GHz, c) 3.1 GHz, d) 4.0 GHz, and e) 5.8 GHz

## 4 Conclusions and Future Work

Simulation results discussed in this paper suggest that reliable communication link between a properly designed on-body directional antenna and an implant located deep in the brain can be achieved from 914 MHz up to 3.1 GHz. Beyond those frequencies, communication depth may be limited. Our evaluations also point to the impact of the on-body antenna location on the propagation depth. When the antenna is located on the top of the head, the gap between the left and the right brain hemispheres (i.e., the great longitudinal fissure) could lead to better signal penetration to the middle of the brain. Existence of a secondary propagation path through the nasal cavity at 5.8 GHz is another phenomenon that could cause stronger than expected signal in the middle of the brain. This would require further studies with several antenna locations and voxel models.

Although, this preliminary study provided some insight into the RF propagation inside the human head, more application-specific research is needed to better understand and characterize the propagation media. The wide spectrum of brain telemetry applications will likely result in a diverse set of wireless connectivity solutions, necessitating multiple propagation channel studies. For brain implants, specialized custom-designed antennas considering regulatory and safety issues as well as SAR limitation for the human brain are needed. These factors will impact the achievable propagation depth at a given frequency. Possibility of using array antennas to create more efficient communication links will also require more in-depth study of the RF propagation inside the human brain. Finally, verification of the simulation results with properly designed head phantoms should also be conducted.

**ACKNOWLEDGMENT**

This work is supported by Academy of Finland 6Genesis Flagship (grant 318927) and the European Union's Horizon 2020 programme under the Marie Sklodowska-Curie grant agreement No. 872752. Mikko Linnanmäki from ExcellAnt is acknowledged for UWB capsule antenna's redesign based in documentation given in [29]. Mikko Parkkila and Uzman Ali from Radientum is acknowledged for mini-horn antenna redesign based on documentation in [28].

## References

1. Chavarriaga R., Cary C., Contreras-Videl J. L., McKinney Z., Bianchi L., "Standardization of Neurotechnology for Brain-Machine Interfacing: State of the Art and Recommendations," in IEEE Open Journal of Engineering in Medicine and Biology, vol. 2, pp. 71-73, 2021.
2. Song Z. et al., "Evaluation and Diagnosis of Brain Diseases based on Non-invasive BCI," 2021 9th International Winter Conference on Brain-Computer Interface (BCI), 2021.
3. L. Song and Y. Rahmat-Samii, "An End-to-End Implanted Brain–Machine Interface Antenna System Performance Characterizations and Development," in IEEE Transactions on

Antennas and Propagation, vol. 65, no. 7, pp. 3399-3408, July 2017, doi: 10.1109/TAP.2017.2700163.

4. W. Chen, C. W. L. Lee, A. Kiourti and J. L. Volakis, "A Multi-Channel Passive Brain Implant for Wireless Neuropotential Monitoring," in IEEE Journal of Electromagnetics, RF and Microwaves in Medicine and Biology, vol. 2, no. 4, pp. 262-269, Dec. 2018
5. Roldan M.et al, “Non-Invasive Techniques for Multimodal Monitoring in Traumatic Brain Injury: Systematic Review and Meta-Analysis, Journal of Neurotrauma, Vol 37., No.23, Nov. 2020.
6. Manoufali M., Bialkowski K., Mobashsher A.T, Mohammed B. and Abbosh A, "In Situ Near-Field Path Loss and Data Communication Link for Brain Implantable Medical Devices Using Software-Defined Radio," in IEEE Transactions on Antennas and Propagation, vol. 68, no. 9, pp. 6787-6799, Sept. 2020.
7. Albert B., Zhang J., Noyvirt A., Setchi R., Sjaaheim H., Velikova S., et al., "Automatic EEG processing for the early diagnosis of traumatic brain injury", 2016 World Automation Congress (WAC), pp. 1-6, 2016, July.
8. Brastad Evensen K, Eide, P. “Measuring Intracranial pressure by invasive, less invasive and non-invasive means, limitations and avenues for improvement,” Fluids and Barrierd of the CNS 17, No. 34, 2020.
9. Imaduddin SM, Fanelli A, Vonberg F, Tasker RC, Heldt T. Pseudo-Bayesian model-based noninvasive intracranial pressure estimation and tracking. IEEE Trans Biomed Eng. 2019.
10. Barone, D G, Czosnyka, M., “Brain Monitoring: Do We Need a Hole? An Update on Invasive and Noninvasive Brain Monitoring Modalities,” The Scientific World Journal., 2014.
11. Särestöniemi M., Pomalaza-Raez C., Hakala J., Myllymäki S., Kilpijärvi J., Iinatti J, Hämäläinen M., Myllylä T.,” Detection of brain hemorrhage in white matter using analysis of radio channel characteristics,” BodyNets2020, Oct. 2020.
12. Hakala J., Kilpijärvi J., Särestöniemi M., Hämäläinen M., Myllymäki S. and Myllylä T., "Microwave Sensing of Brain Water – a Simulation and Experimental Study Using Human Brain Models," in IEEE Access, vol. 8, pp. 111303-111315, 2020, doi: 10.1109/ACCESS.2020.3001867.
13. Patel, P., Sarkar, M. & Nagaraj, S. Wireless channel model of ultra wideband radio signals for implantable biomedical devices. Health Technol. 8, 97–110 (2018).
14. Särestöniemi M, Pomalaza-Raez C., Sayrafian K. Iinatti J., ”In-Body Propagation at ISM and UWB Frequencies for Abdominal Monitoring Applications,” IoT Health Workshop, ICC conference, Montreal, Canada, 2021.
15. Dove I. “Analysis of Radio Propagation Inside the Human Body for in-Body Localization Purposes,” Master Thesis, Faculty of Electrical Engineering, Mathematics and Computer Science, University of Twente, Netherlands, Aug. 2014.
16. A. K. Teshome, B. Kibret and D. T. H. Lai, "A Review of Implant Communication Technology in WBAN: Progress and Challenges," in *IEEE Reviews in Biomedical Engineering*, vol. 12, pp. 88-99, 2019.
17. M. Mohamed, B. J. Maiseli, Y. Ai, K. Mkocha and A. Al-Saman, "In-Body Sensor Communication: Trends and Challenges," in *IEEE Electromagnetic Compatibility Magazine*, vol. 10, no. 2, pp. 47-52, 2nd Quarter 2021.
18. R. Aminzadeh, A. Thielens, M. Zhadobov, L. Martens and W. Joseph, "WBAN Channel Modeling for 900 MHz and 60 GHz Communications," in IEEE Transactions on Antennas and Propagation, vol. 69, no. 7, pp. 4083-4092, July 2021.
19. S. Hout and J. Chung, "Design and Characterization of a Miniaturized Implantable Antenna in a Seven-Layer Brain Phantom," in IEEE Access, vol. 7, pp. 162062-162069, 2019.

20. H. Bahrami, S. A. Mirbozorgi, R. Ameli, L. A. Rusch and B. Gosselin, "Flexible, Polarization-Diverse UWB Antennas for Implantable Neural Recording Systems," in IEEE Transactions on Biomedical Circuits and Systems, vol. 10, no. 1, pp. 38-48, Feb. 2016.
21. B. Rana, J. -Y. Shim and J. -Y. Chung, "An Implantable Antenna With Broadside Radiation for a Brain–Machine Interface," in IEEE Sensors Journal, vol. 19, no. 20, pp. 9200-9205, 15 Oct.15, 2019.
22. D. Nguyen and C. Seo, "An Ultra-Miniaturized Antenna Using Loading Circuit Method for Medical Implant Applications," in IEEE Access, vol. 9, pp. 111890-111898, 2021.
23. E. Moradi, T. Björninen, L. Sydänheimo, J. M. Carmena, J. M. Rabaey and L. Ukkonen, "Measurement of Wireless Link for Brain–Machine Interface Systems Using Human-Head Equivalent Liquid," in *IEEE Antennas and Wireless Propagation Letters*, vol. 12, pp. 1307-1310, 2013.
24. Bahrami H., Mirbozorgi S.A., Rusch L.A, and Gosselin B., "Biological Channel Modeling and Implantable UWB Antenna Design for Neural Recording Systems," in IEEE Transactions on Biomedical Engineering, vol. 62, no. 1, pp. 88-98, Jan. 2015, doi: 10.1109/TBME.2014.2339837.
25. Dassault Simulia CST Suite, https://www.3ds.com/
26. J. Orfanidis, “Electromagnetic Waves and Antennas,” 2002, revised 2016, online: http://www.ece.rutgers.edu/~orfanidi/ewa/.
27. https://www.itis.ethz.ch/virtual-population/tissue-properties/databaseM
28. Blauert J. and Kiourti A, "Bio-Matched Horn: A Novel 1–9 GHz On-Body Antenna for Low-Loss Biomedical Telemetry with Implants," in IEEE Transactions on Antennas and Propagation, vol. 67, no. 8, pp. 5054-5062, Aug. 2019.
29. Shang J. and Yu Y., "An Ultrawideband Capsule Antenna for Biomedical Applications," in IEEE Antennas and Wireless Propagation Letters, vol. 18, no. 12, pp. 2548-2551, Dec. 2019.